Fatigue behavior of reinforced concrete beams strengthened with externally bonded prestressed CFRP sheets

Hui Huang[1], Wen-Wei Wang[2], Jian-Guo Dai[3] and John C. Brigham[4,5]

[1] PhD candidate, Department of Bridge Engineering, Southeast University, Nanjing, China, E-mail: huang871005@126.com

[2] Professor (Corresponding author), Department of Bridge Engineering, Southeast University, Nanjing, China, Tel: 862583792352, Fax: 862583794100, E-mail: wangwenwei@seu.edu.cn

[3] Associate Professor, Department of Civil and Structural Engineering, The Hong Kong Polytechnic University, Hung Hom, Hong Kong, E-mail: cejgdai@polyu.edu.hk

[4] Senior Lecturer, Durham University, School of Engineering and Computing Sciences, Durham, DH1 3LE, UK, E-mail: john.brigham@durham.ac.uk

[5] Associate Professor, Department of Civil and Environmental Engineering, University of Pittsburgh, Pittsburgh, USA

Abstract: An experimental study was conducted to investigate the fatigue behavior of reinforced concrete (RC) beams strengthened with post-tensioned prestressed carbon fiber-reinforced polymer (CFRP) sheets. The experimental program consisted of nine rectangular section simply supported RC beams: four beams were statically tested to failure to determine the values of the fatigue loads to apply, and the remaining five beams were tested under fatigue load. The main purpose of the fatigue tests was to gain a better understanding of the fatigue performance and failure modes of RC beams strengthened with post-tensioned prestressed CFRP sheets. The experimental results indicated that the fatigue failure mode of the prestressed CFRP sheet-strengthened RC beams was tensile steel reinforcement rupture at the main cracked section. Moreover, the fatigue performance of the prestressed CFRP sheet-strengthened RC beams was significantly better than that of both un-strengthened and non-prestressed CFRP sheet-strengthened beams. Finally, a fatigue life prediction model that considers the gradual deterioration of performance of the component materials and partial debonding of the FRP was presented and applied to predict the fatigue life of 28 tested beams with two extreme FRP-to-concrete interfacial states. The results showed that the predicted fatigue life was close to the experimentally measured fatigue life for the fully bonded state. Thus, the effectiveness of the proposed model was verified, and the effect of fatigue-load-induced FRP debonding along the beam substrate on fatigue life prediction was found to be insignificant.

Keywords: Prestressed CFRP sheet; RC beam; Fatigue performance; Steel reinforcement rupture; Fatigue life

Introduction

The application of externally bonded fiber-reinforced polymer (FRP) sheets for strengthening existing reinforced concrete beams/girders has increased during the past several decades. The reason that FRP sheets are so popular for strengthening is because of the high strength/weight ratio, ease of handling and application, the elimination of the need for heavy equipment, a faster construction rate, and the fact that the FRP does not corrode (ACI 2002; Su et al. 2011).

FRP strengthening techniques can be classified into two types according to the initial stress in the FRP material: non-prestressed FRP strengthening and prestressed FRP strengthening (Meier 1995; Saadatmanesh and Malek 1998; Wight et al. 2001; Benachour et al. 2008; Mukherjee and Rai 2009; Kim et al. 2010; El-Hacha et al. 2001; Wang et al. 2012; Wang et al. 2014). Compared with the former technique, the prestressed FRP strengthening provides some distinct advantages (Wight et al. 2001; Benachour et al. 2008; Mukherjee and Rai 2009; Kim et al. 2010; Wang et al. 2012): fully utilizing the high strength of FRP, improving the serviceability of RC beams, limiting the propagation of old cracks, delaying the formation of new cracks, and enhancing the stiffness of RC beams. Based on these advantages of the prestressed FRP technique, various post-tensioned systems (Triantafillou and Deskovic 1991; Nanni et al. 1992; Nanni et al. 1996; Erki and Meier 1999; Ekenel et al. 2006; Sika CarboStress 2014) and relevant prestress levels for FRP in application (Sika CarboDur 2005) have been proposed and extensively used in practice for strengthening structures.

During the past several decades, various experimental and theoretical works (Barnes and Mays 1999; Shahawy and Beitelman 1999; Papakonstantinou et al. 2001; Aidoo et al.

2004; Heffernan et al. 2004; Brena et al. 2005; Gussenhoven and Brena 2005; Larson et al. 2005; Masoud et al. 2005; Quattlebaum et al. 2005; Rosenboom and Rizkalla 2005; Toutanji et al. 2006) have been performed on the fatigue behavior of RC beams strengthened with non-prestressed FRP sheets. In these studies, some experimental results showed that the fatigue performance of FRP-sheet-strengthened RC beams was improved significantly over un-strengthened beams due to the improved beam stiffness with the addition of bonded FRP sheets (Shahawy and Beitelman 1999; Papakonstantinou et al. 2001; Aidoo et al. 2004; Larson et al. 2005; Rosenboom and Rizkalla 2005). Another feature is that the majority of the observable fatigue damage in FRP-sheet-strengthened RC beams was generally accumulated rapidly within the early load cycles (Heffernan et al. 2004; Gussenhoven and Brena 2005; Quattlebaum et al. 2005). In addition, some theoretical studies revealed that the fatigue life of FRP-sheet-strengthened RC beams can be increased when the stress redistribution between the steel and FRP is considered (Masoud et al. 2005; Toutanji et al. 2006). Moreover, some test results (Barnes and Mays 1999; Brena et al. 2005; Chen and Cheng 2016; Charalambidi et al. 2016) showed that the fatigue failure of FRP-strengthened RC beams is governed by tensile steel rupture, rather than the fatigue failure of the component materials (i.e., concrete and the FRP).

Relatively limited work in the literature can be found on the fatigue performances of prestressed FRP-sheet-strengthened RC beams. In the study of Aidoo et al. (2004), the authors conducted fatigue tests on eight T-beams strengthened with prestressed CFRP sheets and found that the fatigue behavior of such retrofitted beams was controlled by the fatigue behavior of the steel reinforcement. Xie et al. (2012) conducted tests on eight rectangular RC beams strengthened with prestressed CFRP sheets and found that all

specimens failed due to tensile steel reinforcement rupturing followed by FRP debonding. The fatigue life of the strengthened beams increased due to the reduction in the steel stress caused by the externally bonded prestressed CFRP sheet. Wight et al. (2003) conducted a cyclic load test on a series of RC slabs strengthened with non-prestressed and prestressed CFRP sheets. The test results showed that the fatigue life of strengthened RC slabs with CFRP sheets, especially prestressed CFRP sheets, increased significantly.

Although the above-referenced works have explored some aspects of the fatigue performance of prestressed CFRP-sheet-strengthened RC elements, there remain several points that are not yet clearly understood, especially relating to the prediction of the fatigue life of such strengthened members. The main objectives of this paper are 1) to extend the experimental fatigue database of prestressed FRP-strengthened RC beams, 2) to present a fatigue life prediction model that considers the gradual deterioration of the performance of the component materials and the partial debonding of the FRP, and 3) to investigate thoroughly the failure mode and failure process, especially concerning FRP debonding near the main cracked section of such strengthened RC beams.

Experimental program

Post-tensioned system

In the present work, a post-tensioned system that was applied successfully in a previous monotonic experiment (Wang et al. 2012) for CFRP sheets was adopted, as shown in Fig. 1. This system included two end anchorages (i.e., a pulled-end anchorage and a fixed-end anchorage), tensioning equipment, a steel frame and a series of bolts. The anchorages at the tensioned and fixed ends were two steel plates, which clamped the impregnated CFRP

sheet tightly by tightening four bolts. The tensioning equipment included a load sensor used to monitor the variation in the prestress force at the tensioned end and a hydraulic oil jack for applying the prestress. The detailed procedure for applying the prestressing forces to the CFRP sheet can be found in the study of Wang et al. (2012).

Test specimens

Nine specimens were tested in this experiment: four beams were tested under monotonic loading to determine the load carrying capacity, and five beams were tested under fatigue loading to observe the fatigue performance. All beams had the same sectional dimensions (i.e., 150 mm width and 300 mm depth) and were simply supported on two roller supports with a span of 1800 mm. Two-point symmetrical loading was applied on the top face of each beam to form a 600 mm pure flexural region, as shown in Fig. 2. Seven days of epoxy resin cure were followed by the application of the CFRP sheet for the strengthened specimens. All beams were placed in an environmental chamber at a controlled temperature of 20±2°C and relative humidity (RH) maintained between 55% and 60% for approximately three months to allow the concrete to shrink freely before testing.

Specimens SB-1 and FB-1 were un-strengthened reference beams, and the remaining specimens (SB-2, SB-3, SB-4, FB-2, FB-3, FB-4 and FB-5) were all strengthened with externally bonded CFRP sheets with varying prestress levels and number of layers (as specified in Table 1). Among these strengthened specimens, beams SB-2 and FB-2 were strengthened with one ply of non-prestressed CFRP sheets; beams SB-3, FB-3 and FB-4 were externally bonded with one ply of prestressed CFRP sheets; and beams SB-4 and

140 FB-5 were strengthened with two plies of prestressed CFRP sheets. The initial prestress
141 for specimens SB-3, FB-3 and FB-4 was 60% of the ultimate tensile strength of the CFRP
142 sheets, and 30% of the ultimate tensile strength of the CFRP sheets was used for beams
143 SB-4 and FB-5. The upper limit of the fatigue load was set to be 40%-50% of the
144 ultimate load-carrying capacity of the specimens (P_u). This upper limit of the fatigue load
145 range represents the possible live load acting on typical simply supported RC bridge
146 girders according to the Chinese bridge design specifications [Ministry of Transport of
147 the People's Republic of China (MTPRC) 2004]. The lower limit of the fatigue load
148 varied from 12%-15% of the ultimate load-carrying capacities to ensure that each
149 specimen has the same stress ratio (P_{min}/P_{max}) of 0.3. The notations P_{min}, P_{max} and P_u are
150 defined as the lower limit of the fatigue load, the upper limit of the fatigue load, and the
151 ultimate load, respectively.

152 ***Material properties***

153 The cube compressive strength of concrete was measured as 52.4 MPa by averaging three
154 cube coupons with a side length of 150 mm. Two deformed bars with a diameter of 14
155 mm were placed in the bottom portion of the beam to serve as the tensile steel
156 reinforcement, and two bars with the same diameter were placed in the top portion of the
157 beam to serve as the compressive steel reinforcement. To prevent shear failure from
158 occurring prematurely, 8 mm in diameter round steel bars were set in the shear span
159 region with a center-to-center spacing of 50 mm. From the results of the bar tensile tests,
160 the measured values of the yield strength and elastic modulus were found to be 335 MPa
161 and 200 GPa, respectively, for the 14 mm deformed steel bar and 280 MPa and 210 GPa,
162 respectively, for the 8 mm round steel bar. The strengthening material was unidirectional

163 CFRP sheets manufactured by HITEX cooperation. The CFRP sheets had a length of
164 1450 mm, a width of 140 mm, and a thickness of 0.167 mm; the measured mean value of
165 the tensile strength was 3522 MPa, with a standard deviation of 157.2 MPa; and the
166 elastic modulus was 258.9 GPa, with a standard deviation of 12.5 GPa. A two-component
167 epoxy resin was evenly brushed on the bottom face of the strengthened beams with a 2
168 mm thickness. The tensile strength, elastic modulus, and shear strength of the epoxy resin
169 were 40.2 MPa, 2.77 GPa, and 16.2 MPa, respectively.

170 ***Test setup and test procedure***

171 Six vibrating wire strain gauges were attached to the concrete face along the depth of
172 each beam with a 50 mm spacing to monitor the development of concrete strain at the
173 mid-span section during the cyclic loading. Two resistance strain gauges were attached to
174 both the tensile steel reinforcement and CFRP sheets at the mid-span section to measure
175 the variations and development of the strains in the two materials. Three dial indicators
176 were placed on the mid-span section and on two supports to monitor their deflections. A
177 load cell was used to monitor the applied loads. Figure 3 shows a picture of the test setup
178 for the fatigue tests.

179 The applied load was a sinusoidal dynamic load with a frequency of 4 Hz, which was
180 applied on the beams using a MTS fatigue machine with a capacity of 200 kN. The
181 deflections and strains of the concrete, steel, and CFRP sheets were measured by the
182 specified instruments, and the propagation of flexural and shear cracks was observed
183 when the fatigue loading terminated at the first cycle, 100,000th cycle, and up to the

184 2,000,000th cycle in intervals of 500,000 cycles. All experiments were terminated at a
185 maximum of 2,000,000 load cycles, regardless of whether failure occurred.

186 ## Experimental results and discussion

187 ***Static tests***

188 Before the fatigue test, four beams (i.e., SB-1, SB-2, SB-3 and SB-4) were tested under
189 monotonic loading to determine the magnitude of the loads to apply for the fatigue
190 specimens according to their ultimate loads P_u. Different failure modes were presented in
191 the four un-strengthened and strengthened beams. Reference beam SB-1 was controlled
192 by a typical flexural failure, with concrete crushing in the compressive zone after the
193 tensile reinforcement steel yielded. For beam SB-2, which had one layer of
194 non-prestressed CFRP sheets, the CFRP sheet ruptured after partial debonding near the
195 main flexural crack; subsequent crushing of the concrete in the compression zone
196 occurred. For beam SB-3, which was strengthened with one layer of post-tensioned
197 CFRP sheets, the fracturing of individual fibers was observed, followed by complete
198 rupture of the CFRP sheet near the mid-span section. For beam SB-4, which was
199 strengthened with two layers of post-tensioned CFRP sheets, failure was observed as
200 simultaneous concrete crushing and brittle rupture of the CFRP sheets.

201 Without CFRP sheet strengthening, specimen SB-1 had the lowest cracking load, 17.6 kN,
202 of all monotonically tested specimens. For beam SB-2, which was strengthened with one
203 layer of non-prestressed CFRP, and beam SB-3, strengthened with one layer of
204 prestressed CFRP, the cracking loads were 23.3 kN and 35.7 kN, respectively,
205 representing an increase compared to SB-1 of 32.3% and 102.8%, respectively. This

206 increase in cracking load demonstrated the effect of the pre-compression at the bottom
207 face of the beam resulting from the pre-tensioning action. Alternatively, the cracking load
208 of SB-4 (44.5 kN) was higher than that of SB-3 due to the increased number of CFRP
209 layers for strengthening. For the ultimate loads, the non-strengthened beam, SB-1, and
210 the CFRP strengthened beams, SB-2, SB-3, and SB-4, were experimentally observed to
211 achieve ultimate loads of 47.3, 77.9, 85.3, and 115.0 kN, respectively, as shown in Table
212 1. Compared with the un-strengthened beam, SB-1, the load-carrying capacities of the
213 strengthened beams, SB-2, SB-3, and SB-4, were increased by 65%, 80%, and 145%,
214 respectively.

215 Figure 4 shows the applied load versus mid-span displacement responses of all
216 monotonically tested beams. As can be observed from Fig. 4, the load-displacement
217 curve of beam SB-1 experienced three stages, which reflected the variations in the
218 flexural stiffness: the initial non-cracked stage, the cracked stage, and the yielded tensile
219 reinforcement stage. Moreover, all strengthened beams (i.e., SB-2, SB-3 and SB-4)
220 showed higher flexural stiffness compared to the control beam, SB-1, in the last two
221 stages after concrete cracking. Comparing the two strengthened beams, the displacement
222 of SB-2, with non-prestressed CFRP, was larger than that of SB-3, with prestressed
223 CFRP. A similar phenomenon can be found in the comparison between beams SB-3 and
224 SB-4. It is clear that introducing the prestressing force into the CFRP sheets and
225 increasing the number of CFRP sheet layers can effectively enhance the flexural stiffness
226 and improve the serviceability of the strengthened beams.

227 ***Fatigue tests***

228 *Failure modes*

229 No fatigue failure was observed in beams FB-1, FB-2, and FB-3 after 2 million loading
230 cycles. However, fatigue failure in the form of CFRP sheet rupture for beam FB-4 and
231 complete CFRP sheet debonding from the bottom face for beam FB-5 were observed
232 following tensile steel reinforcement rupturing at the 1,730,000th and 1,890,000th load
233 cycles, respectively, as shown in Fig. 5.

234 The observed failure processes of the two beams (i.e., FB-4 and FB-5) could be divided
235 into the following three stages: (1) The crack propagation stage. During this stage,
236 bending and shearing cracks appeared in the pure flexural and flexural-shear regions of
237 the beams, and one of these cracks rapidly developed into the main crack. The CFRP
238 sheet-to-concrete interface around the main cracked section was damaged (i.e., FRP sheet
239 partial debonding) due to the stress concentration at the root of the cracks, as shown in
240 Fig. 6. Although this first stage constitutes no more than 10% of the total fatigue life, a
241 rapid development of the cracks was observed, as shown in Fig. 7. (2) The damage
242 accumulation stage. After the first stage, the change in observable fatigue damage
243 became minimal for a long period of time. The increment in the number of cracks, the
244 development of the maximum crack length, and the maximum crack width all remain
245 approximately constant, as shown in Fig. 7. This second stage constitutes more than 90%
246 of the total fatigue life, and minimal degeneration of the flexural stiffness was observed.
247 (3) The failure stage. After substantial fatigue damage accumulation, the tensile steel
248 reinforcement ruptured at the main cracked section. Then, the tensile force carried by the
249 steel reinforcement was transferred to the CFRP sheet, which led to a sudden increase in

the tensile stress in the CFRP sheet. The increase in tensile stress resulted in the fracture of the CFRP sheet for beam FB-4 and the complete debonding of the CFRP sheets from the concrete subsurface for beam FB-5. Simultaneously, the concrete was crushed at the compression zone due to the relatively fast propagation of the main crack. This final stage lasted a relatively short time.

Crack development and mid-span deflection

During the fatigue loading process, the propagation and development of flexural and shear cracks in each specimen were recorded at each previously specified benchmark number of load cycles. Figure 8 shows the distribution of cracks on the surface of one side of the beams at the various numbers of loading cycles. All strengthened beams showed more cracks and a smaller crack spacing when compared to un-strengthened reference beam FB-1. For beams FB-2 and FB-3 with the same fatigue range but different prestress levels, the number of cracks increased and the spacing of the cracks decreased due to the additional prestress for beam FB-3. Moreover, the number of CFRP sheets also affected the distribution of cracks significantly, as seen from the two beams FB-4 and FB-5 with the same fatigue range and equivalent initial tensile force in the CFRP sheets. The larger number of cracks and smaller crack spacing for beams strengthened with prestressed CFRP sheets are believed to be attributed to the 'bridging actions' of the prestressed CFRP sheets in the process of crack formation and development. Higher prestress induced into the CFRP sheets and more CFRP reinforcement bonded to the bottom surface of an RC beam increases the depth of the concrete compressive zone, resulting in an increase in the number of cracks and a decrease in the crack spacing.

Figure 9 shows the relationships between the mid-span deflection and the number of load cycles at the same load of 19.8 kN for all fatigue specimens. This given load was equal to the upper limit of the fatigue load for reference beam FB-1. As can be observed from Fig. 9, different specimens presented different mid-span deflections under the same given load. Among all fatigue-loaded specimens, beam FB-5, strengthened with two layers of prestressed CFRP sheets, presented the minimum mid-span deflection, and the un-strengthened beam FB-1 showed the maximum mid-span deflection. The mid-span deflections of the beams strengthened with one layer of prestressed CFRP sheets (FB-3 and FB-4) were significantly smaller than those of the beam strengthened with one layer of non-prestressed CFRP sheets (FB-2).

Apart from the mid-span deflections, different specimens showed different increments of mid-span deflections when the load cycle benchmarks were reached. Compared with the un-strengthened beam FB-1, all CFRP-sheet-strengthened beams presented lower increments of the mid-span deflection. For example, beam FB-1 had a deflection increment of 0.10 mm when 1.5 million load cycles was reached. The corresponding increments for FB-2, FB-3, FB-4, and FB-5 were only 0.05, 0.03, 0.03, and 0.02 mm, respectively. The differences in the deflection increments for all strengthened beams were mainly caused by the differences in the strengthening methods. An externally bonded CFRP sheet with initial prestressing or greater thickness can limit the propagation of cracks and enhance the flexural stiffness; therefore, the fatigue performance of such beams can be improved significantly with these strengthening methods.

293 *Strain response*

294 Figure 10 shows the distribution of the mid-span sectional strain for the strengthened
295 beam FB-3 under a load of 34.1 kN, which is the upper limit of the fatigue load for FB-3,
296 at the various levels of load cycles. Since the lower strain gauge attached to the side face
297 of the strengthened beam was damaged after the 100,000th load cycle, the value of this
298 stain gauge was unavailable after that point. As seen in Fig. 10, an approximately linear
299 strain distribution was observed from the 1st load cycle to the 2,000,000th load cycle. The
300 depth of the concrete compression zone decreased, while the strain values (absolute value
301 of the compressive strain) of each measurement point increased gradually.

302 Figure 11 shows the relationships between the compressive strains of the concrete
303 attached to the top face of the fatigue loaded beams, the tensile steel reinforcement strains,
304 and the CFRP sheet strains with respect to the number of load cycles at the given load of
305 19.8 kN. As shown in Fig. 11a, the strains in the steel reinforcement in all specimens
306 experienced a significant increase with increasing load cycles before the cycle number
307 reached 100,000 and then increased more slowly during the remaining load cycles. The
308 same behavior was observed in the developments of the concrete and CFRP sheet strains,
309 as shown in Fig. 11b and Fig. 11c, respectively.

310 Although a similar variation trend can be found in the strains for all component materials,
311 the rate of the strain increments were different depending on the particular component
312 material. For example, the rate of increment of the concrete strains were 24.72%, 14.7%,
313 8.64%, 9.7%, and 5.73% for beams FB-1, FB-2, FB-3, FB-4, and FB-5, respectively, at
314 the 1,500,000th cycle compared to the strains at the first cycle. The differences in the rate

315 of strain increment are caused by the differences in the prestress level, fatigue loading
316 range, and CFRP sheet reinforcement. Although beams FB-1, FB-2, and FB-3 had the
317 same fatigue loading range, the growth ratio of the concrete strain in beam FB-3 obtained
318 the minimum value. The minimum value of the concrete strain for FB-3 is because the
319 propagation of the concrete cracks is limited by the externally bonded layer of prestressed
320 CFRP sheets. Moreover, the number of CFRP sheet layers also affects the rate of
321 increment of the concrete strains. Due to the one additional layer of CFRP sheets in FB-5,
322 the concrete strain in FB-5 was significantly smaller than that of FB-4, as seen in Fig.
323 11b.

324 Predictive model of fatigue life

325 As observed from the fatigue test results, rupture of the tensile steel reinforcement at the
326 main cracked section was the controlling failure mode for the prestressed CFRP
327 sheet-strengthened RC beams under fatigue loading. This behavior has also been widely
328 observed in RC beams strengthened with non-prestressed FRP sheets in the related
329 literature (Barnes and Mays 1999; Papakonstantinou et al. 2001; Heffernan et al. 2004;
330 Quattlebaum et al. 2005; Toutanji et al. 2006; Yu et al. 2011; Xie et al. 2012). Therefore,
331 the fatigue life (i.e., the number of load cycles) of non-prestressed and prestressed FRP
332 sheet-strengthened RC beams can be determined according to the fatigue life of the
333 tensile steel reinforcement. In this section, an analytical model for predicting the fatigue
334 life of non-prestressed and prestressed FRP sheet-strengthened RC beams is proposed
335 based on Miner's rule (Miner 1945) and the sectional analysis method (Wang and Dai
336 2013; Wang et al. 2013). In addition, the gradual performance deterioration of the
337 component materials with increasing load repetitions and the FRP-to-concrete interfacial

state are both considered in fatigue life prediction.

Fatigue damage of tensile steel reinforcement

The accumulated fatigue damage of the tensile steel reinforcement can be calculated using Miner's rule:

$$D = \sum \frac{n_i}{N_i} \tag{1}$$

where D is the consumed fatigue resistance ($D \leq 1$), n_i is the specified number of repetitions for the specified stress amplitude σ_{si}, and N_i is the corresponding number of repetitions to failure for the stress amplitude σ_{si}. The relationship between N_i and σ_{si} for deformed and smooth steel reinforcement is given as (BS5400 1978)

$$N_i \sigma_{si}^k = K_0 \Delta^d \tag{2}$$

where k is the inverse slope of the mean-line $\log\sigma_{si}$-$\log N_i$, K_0 is a constant term relating to the mean-line of the statistical analysis results, □ is the reciprocal of the anti-log of the standard deviation of $\log N_i$, and d is the number of standard deviations below the mean-line. The values of these terms with the mean-line relationship are shown in Table 2.

Using the determined fatigue damage of the tensile steel reinforcement, the fatigue life of FRP-sheet-strengthened RC beams can be predicted by the summation of the corresponding fatigue load cycles of each stress amplitude until rupture failure of tensile steel reinforcement occurs (i.e., D=1):

$$N_p = \sum n_i \tag{3}$$

where N_p is the predicted fatigue life.

359 ***Determining stress amplitudes of tensile steel reinforcement***

360 For an FRP-sheet-strengthened RC beam under constant fatigue loading, the stress
361 amplitude of the tensile steel reinforcement changes continuously with increasing load
362 cycles due to the generation and propagation of flexural and shearing cracks and the
363 deterioration of the material performance (ACI 1997), as shown by the dotted line in Fig.
364 12. To simplify the nonlinear stress amplitude curve-induced complexity in the fatigue
365 life prediction, a discretization method was adopted to divide the curve into many
366 constant loading blocks (i.e., each block having the same number of load cycles), and the
367 stress amplitude was assumed to be unchanged within each specific loading block. From
368 Fig. 12, note that there is a large gap between the supposed stress amplitude and the
369 actual stress amplitude in the first few loading blocks (i.e., the crack propagation stage)
370 when ignoring the gradual development of cracks. Since the crack propagation stage is
371 short relative to the total fatigue life, the gap-induced error in the lifetime prediction can
372 be ignored.

373 Based on the aforementioned discretization method, the sectional analysis method can be
374 adopted to calculate the maximum and minimum stresses generated in the tensile steel
375 reinforcement for each loading block. With the sectional analysis method, the
376 fatigue-load-induced concrete strain and steel strain can be determined with the
377 assumption of a linear strain distribution, as seen in Fig. 13. In contrast, the FRP strain
378 cannot be determined with the same assumption because the fatigue-load-induced
379 FRP-concrete interface damage (i.e., partial debonding) causes a loss of deformation
380 compatibility between the FRP sheet and the concrete substrate. The fatigue-load-induced
381 FRP strain will be addressed in the following section separately. Then, based on the

sectional equilibriums of external and internal forces and moments, the following equations can be expressed:

$$P = E_s \varepsilon_{sn} A_s + E_f (\varepsilon_{fn} + \varepsilon_{pe}) A_f - \int_0^{x_n} E_{cn} [\varepsilon_{cn}(y) - \varepsilon_{cn,c}(y)] b dy - E_s' \varepsilon_{sn}' A_s' \quad (4)$$

$$M = E_s \varepsilon_{sn} A_s (h - c_n - a) + E_f (\varepsilon_{fn} + \varepsilon_{pe}) A_f (h - c_n) + \int_0^{x_n} E_{cn} [\varepsilon_{cn}(y) - \varepsilon_{cn,c}(y)] b y dy + E_s' \varepsilon_{sn}' A_s' (c_n - a') \quad (5)$$

where P is the axial force (for a simply supported beam: P=0); M is the bending moment induced by external actions at the main cracked section; c_n is the depth of the compression zone for the concrete at the n^{th} cycle at the main cracked section; E_s', E_s and E_f are the elastic modulus of the compressive steel reinforcement, tensile steel reinforcement and FRP, respectively; E_{cn} is the effective elastic modulus of the concrete at the n^{th} cycle; ε_{sn}' and ε_{sn} are the longitudinal strains at the centroid of the compressive steel reinforcement and tensile steel reinforcement, respectively; ε_{fn} is the FRP strain caused by the fatigue load; ε_{pe} is the initial-prestress-induced FRP strain; $\varepsilon_{cn}(y)$ and $\varepsilon_{cn,c}(y)$ are the total strain and creep strain of the specified concrete layer at the n^{th} cycle; A_s', A_s and A_f are the cross sectional areas of the compressive steel reinforcement, tensile steel reinforcement and FRP, respectively; b is the beam width; a' is the distance from the center of the compressive steel reinforcement to the top surface; a is the distance from the center of the tensile steel reinforcement to the subsurface; and y is the distance between the centroid of the specified concrete layer and the neutral axis.

Using an iterative approach and combining Eqs. (4) and (5), the maximum and minimum stresses generated in the tensile steel reinforcement can be obtained by substituting the corresponding maximum and minimum moments into Eq. (5). With the calculated maximum and minimum stresses, the stress amplitude of the tensile steel reinforcement

404 can be determined according to the following equation:

405 $$\sigma_{si} = \sigma_{sn,\max} - \sigma_{sn,\min} \tag{6}$$

406 where $\sigma_{sn,\max}$ and $\sigma_{sn,\min}$ are the maximum and minimum stresses generated in the tensile
407 steel reinforcement, respectively.

408 ***Time-dependent constitutive relationships of component materials***

409 To obtain the maximum and minimum stresses of the tensile steel reinforcement
410 accurately, the time-dependent constitutive relationships of all the component materials
411 should be considered within the analytical model. The experimental results of Holmen
412 (1982) showed that the compressive stress-strain relationship of concrete changed
413 continuously with repeated fatigue loading due to the internal damage accumulation of
414 the concrete, as shown in Fig. 14. The effective elastic modulus of concrete after a certain
415 number of load cycles n can be written as (Sherif et al. 2001)

416 $$E_{cn} = (1 - 0.33\frac{n}{N_f})E_c \tag{7}$$

417 where E_{cn} is the effective elastic modulus of concrete, n is the number of fatigue load
418 cycles, E_c is the initial elastic modulus of concrete, and N_f is the number of load cycles to
419 failure for concrete, which can be calculated using the following equation (Holmen
420 1982):

421 $$\log N_f = 1.978 S_{\max}^{-3.033}(-\log K)^{0.0596} \tag{8}$$

422 where $S_{\max}$ is the maximum stress level and $S_{\max}=\sigma_{c,\max}/f_c$, f_c is compressive strength of
423 the concrete prism, and K is defined by $K=1-p$, in which p is the probability of failure,
424 $p=0.5$ (Holmen 1982).

On the other hand, the total concrete strain (ε_{cn}) during the fatigue load consists of two parts, elastic strain ($\varepsilon_{cn,\,e}$) and inelastic strain ($\varepsilon_{cn,\,c}$):

$$\varepsilon_{cn} = \varepsilon_{cn,e} + \varepsilon_{cn,c} \tag{9}$$

Based on experimental data, Holmen (1982) proposed the following expressions to calculate the total concrete strain during fatigue loading:

$$\varepsilon_{cn} = \begin{cases} \dfrac{1\times10^{-3}}{tg\alpha}\left|S_{\max} + 3.180(1.183 - S_{\max})\left(\dfrac{n}{N_f}\right)^{0.5}\right| + 0.413\times10^{-3}S_c^{1.184}\ln(t+1) & for\ 0 < \dfrac{n}{N_f} \le 0.1 \\ \dfrac{1.11\times10^{-3}}{tg\alpha}\left|1 + 0.677\left(\dfrac{n}{N_f}\right)\right| + 0.413\times10^{-3}S_c^{1.184}\ln(t+1) & for\ 0.1 < \dfrac{n}{N_f} \le 0.8 \end{cases} \tag{10}$$

where $tg\alpha$ is the secant modulus of concrete ($tg\alpha=S_{\max}/\varepsilon_0$); ε_0 is the concrete strain caused by the upper limit of the fatigue load at the first cycle; S_c is the characteristic stress level and is given as $S_c=S_m+RMS$; t is the duration of the fatigue load (units of hours); S_m is the mean stress level, where $S_m=(S_{\max}+S_{\min})/2$; $S_{\min}$ is the minimum stress level, where $S_{\min}=\sigma_{c,\,m\min}/f_c$; and RMS is the root mean square value of the characteristic stress level for sinusoidal loading, where $RMS=(S_{\max}+S_{\min})/2\sqrt{2}$.

Although repeated loading on the steel reinforcement causes the accumulation of fatigue damage, Barsom et al. (1987) and Rösler et al. (2007) both demonstrated that the elastic modulus of steel reinforcement remains unchanged until immediately before failure, and no significant plastic deformation was observed from the action of high cycle fatigue loading. Moreover, test results in Hull's (1981) research suggested that the mechanical behavior of FRP sheets was virtually unaffected by fatigue loading. Hence, the constitutive relationships of steel reinforcement and FRP sheets are considered to be identical to the initial stress-strain relationships for each loading block.

445 ***Determining strain of FRP sheets***

446 The aforementioned sectional analysis method can be used to calculate the stress
447 amplitude of the tensile steel reinforcement provided that the strain of the FRP sheet was
448 known. However, it is very difficult to calculate precisely the FRP sheet strain because of
449 many influencing factors, particularly the properties of the interface bond between the
450 concrete substrate and the FRP sheet. To simplify the analysis, a limit analytical method
451 is presented to attempt to establish the relationship between the FRP sheet stain and the
452 fatigue life of the strengthened beams. In this method, two extreme FRP-to-concrete
453 interfacial states, the fully bonded state (i.e., the debonding length L_d is equal to 0) and
454 the fully debonding state (i.e., the debonding length L_d is equal to the length of the FRP
455 sheet L_f), were considered to determine which state is closer to the actual situation (e.g.,
456 partial debonding of the FRP sheet at the main cracked section, as shown in Fig. 15).
457 For the fully bonded state, the strain along the depth of the strengthened beam is
458 completely compatible, and the plane section assumption can be used to calculate the
459 FRP sheet strain. Therefore, the FRP sheet strain at the main cracked section can be
460 determined with:

461 $$\varepsilon_{fn} = \frac{h - c_n}{x_n} \varepsilon_{cn} \tag{11}$$

462 When full debonding of the FRP sheet occurs, the strain compatibility across the
463 FRP-concrete interface has been lost, and the FRP sheet strain cannot be determined
464 using the assumption of a plane section. In this case, the FRP sheet behaves as an
465 un-bonded steel tendon with two end anchorages (as seen in Fig. 15). Assuming that the
466 total elongation of the FRP material along the length of the FRP sheet is equal to that of

467 the adjacent concrete, it can be deduced as

468 $$\Delta_f = \Delta_c = \int_{-\frac{L_f}{2}}^{\frac{L_f}{2}} \varepsilon_{cbn} dx \tag{12}$$

469 where L_f is the length of the FRP sheet; Δ_f and Δ_c are the elongation of the FRP sheet and
470 the adjacent concrete, respectively; and ε_{cbn} is the strain of the concrete adjacent to the
471 FRP sheet.

472 For an un-bonded FRP sheet, the stain has a uniform distribution along the length of the
473 FRP sheet; therefore, the FRP strain at the main cracked section can be given as Eq. (13)
474 by averaging the total elongation of the FRP sheet.

475 $$\varepsilon_{fn} = \frac{\int_{-\frac{L_f}{2}}^{\frac{L_f}{2}} \varepsilon_{cbn} dx}{L_f} \tag{13}$$

476 If the bending moment at any section is known, the strain of the concrete adjacent to the
477 FRP sheet can be calculated as

478 $$\varepsilon_{cbn} = \frac{M(x)(h - c_n)}{E_{cn} I_{cn}} \tag{14}$$

479 where $M(x)$ is the bending moment at the section, I_{cn} is the moment of inertia of the RC
480 beam, and c_n is the depth of the concrete compression zone.

481 ***Procedure to estimate the fatigue life***

482 The detailed procedure for predicting the fatigue life is as follows:

483 1. Use Eq. (4) and Eq. (5) to calculate the initial maximum and minimum stresses of
484 the concrete with the applied maximum and minimum fatigue loads. Initially, the
485 elastic modulus of concrete is E_c, and the creep strain of each concrete layer is zero.

2. Substitute these stresses into Eqs. (7)-(10) to build the constitutive model for concrete. These constitutive models are assumed to represent the fatigue behavior during the whole process of the fatigue loading.

3. With the constitutive models, the sectional analysis at the main cracked section is conducted to calculate the maximum and minimum stresses and the stress amplitude of the tensile steel reinforcement in the each loading block using Eqs. (4)-(6).

4. Substitute the value of the stress amplitude of the tensile steel reinforcement into Eq. (1) and Eq. (2) to calculate the fatigue damage of the tensile steel reinforcement for each loading block and further obtain the total accumulated fatigue damage.

5. Adjust the constitutive model for concrete at the end of the last loading block; then, the corresponding stress amplitude and fatigue damage of the steel reinforcement in the next loading block can be calculated using the same method (i.e., sectional analysis).

6. Repeat Steps 3-5 until the total fatigue resistance is consumed, and then, the fatigue life can be obtained after summing the numbers of each loading block using Eq. (3).

The above described procedure was implemented in a MATLAB-based computer program.

Model verification

To investigate the relationship between the FRP strain and fatigue life, an experimental database consisting of 28 prestressed or non-prestressed FRP sheet-strengthened RC beams (Barnes and Mays 1999; Papakonstantinou et al. 2001; Heffernan et al. 2004;

508 Quattlebaum et al. 2005; Toutanji et al. 2006; Yu et al. 2011; Xie et al. 2012) was
509 established. All beams were reported to have failed with the rupture of the tensile steel
510 reinforcement. Those specimens that failed with other modes or that did not include
511 essential parameters were not included in the database. Table 3 summarizes the beam ID
512 and the material parameters for all 28 specimens. In the table, the notations P_{max}, P_{min} and
513 P_u denote the corresponding maximum and minimum fatigue load and the ultimate load,
514 respectively. The notations E_c, E_s and E_f represent the elasticity modulus of the concrete,
515 tensile steel reinforcement and FRP sheet, respectively. The notations N_t, N_{pu} and N_{pd}
516 represent the tested life and the predicted life corresponding to L_d =0 and L_d = L_f,
517 respectively. All selected beams had a rectangular section and were simply supported on
518 the two roller supports. Four-point or three-point fatigue loading was applied to the top
519 face of the strengthened beams. The fatigue life of each specimen was predicted twice
520 under two extreme cases (i.e., L_d=0 and L_d=L_f). The aforementioned fatigue life
521 predictive model was implemented in loading blocks, with each loading block containing
522 10,000 load cycles (i.e., n_c=10,000 cycles).

523 Figures 16a and 16b show the comparisons between the predicted fatigue life N_p and the
524 tested fatigue life N_t for all 28 beams in the databases for the two bond limit states
525 specified. The predicted fatigue lives were obtained based on the presented model after
526 determining the FRP sheet strain using Eq. (11) and Eq. (13). It can be seen that the
527 predicted fatigue lives of all strengthened beams based on the assumption of L_d=0 are
528 evenly distributed around the line of N_{pu}/N_t=1. The average ratio of the predicted life to
529 the tested life (i.e., N_{pu}/N_t) is 1.02, and the corresponding coefficient of variation (COV)
530 is 0.25 (as seen in Table 3). However, the assumption of L_d=L_f leads to a significant

underestimation of the fatigue lives. The average ratio of the predicted life to the tested life (i.e., N_{pd}/N_t) is 0.69, and the corresponding COV is 0.28 (Table 3). Therefore, the predicted results are substantially closer to the test results when the fully bonded state (i.e., L_d=0) is used. This behavior was consistent with the research results from Sherif et al. (2001), in which linear strain distribution along the beam section was assumed for fatigue performance evaluation of FRP-strengthened RC beams. This also demonstrates that localized partial debonding of the FRP sheets at the main cracked section is insignificant when analyzing the fatigue life of FRP-strengthened RC beams.

Conclusions

An experimental study focused on investigating the fatigue behavior of RC beams strengthened with post-tensioned prestressed CFRP sheets was presented. The variables in the experimental program were the prestress level, fatigue load amplitude, and number of CFRP sheets. Moreover, a fatigue life prediction model that considers the gradual deterioration of performance of the component materials was presented and applied to predict the fatigue life of 28 tested beams considering two extreme FRP-to-concrete interfacial states. Based on the comparison between the predicted values and the experimental ones, the effectiveness of the proposed model was verified. The following conclusions can be drawn from the experimental and theoretical results presented in this paper:

1. The static tests showed that the flexural stiffness and the load-carrying capacity of the beams increased with increasing prestress level and number of CFRP sheets; however, the ductility of the reference beam (i.e., the un-strengthened beam) was better than that of the beams with externally bonded CFRP sheets.

554 2. Three distinct stages were observed during the fatigue loading process for
555 prestressed CFRP sheet-strengthened RC beams. The mid-span deflections, material
556 strains and crack development of prestressed CFRP sheet-strengthened beams
557 significantly increased in early loading cycles, which was followed by a long stage
558 with significantly slower development before final failure occurred.

559 3. The typical fatigue failure mode of the prestressed CFRP sheet-strengthened RC
560 beams was tensile steel reinforcement rupture at the main cracked section, followed
561 by CFRP sheet debonding/rupture. This mode was essentially the same as the
562 commonly observed fatigue failure mode of beams strengthened with
563 non-prestressed FRP sheets.

564 4. The theoretical results showed that the predicted fatigue lives are close to the
565 tested lives when the FRP sheet is fully bonded. Thus, the effect of
566 fatigue-load-induced FRP debonding along the beam substrate on fatigue life
567 prediction is insignificant.

568 ## Acknowledgements

569 The authors would like to thank the National Natural Science Foundation of China
570 (Program Nos. 51578135 and 51278441) and the Major State Basic Research
571 Development Program of China (973 Program) (No. 2012CB026201) for providing funds
572 for this research work. In addition, the authors wish to thank the University of Pittsburgh
573 and Durham University for the research collaboration opportunity.

References

Aidoo, J., Harries, K. A., and Petrou, M. F. (2004). "Fatigue behavior of carbon fiber reinforced polymer-strengthened reinforced concrete bridge girders." *J. Compos. Constr.*, 8(6), 501-509.

American Concrete Institute (ACI). (2002). "Guide for the design and construction of externally bonded FRP systems for strengthening concrete structures." *ACI 440.2-02*, Farmington Hills, MI.

Barnes, R. A., and Mays, G. C. (1999). "Fatigue performance of concrete beams strengthened with CFRP plates." *J. Compos. Constr.*, 3(2), 63-72.

Barsom, J. M., and Rolfe, S. T. (1987). *Fracture and Fatigue Control in Structures*, Prentice Hall, Englewood Cliffs, N.J.

Benachour, A., Benyoucef, S., Tounsi, A., and Adda bedia, E. A. (2008). "Interfacial stress analysis of steel beams reinforced with bonded prestressed FRP plate." *Eng. Struct.*, 30(11), 3305-3315.

Brena, S. F., Benouaich, M. A., Kreger, M. E., and Wood, S. (2005). "Fatigue tests of reinforced concrete beams strengthened using carbon fiber-reinforced polymer composites." *ACI Struct. J.*, 102(2), 305-313.

BS5400. (1978). "Steel, concrete and composite bridges-part 10: code of practice for fatigue." *British Standards Institution*, London, U.K.

Charalambidi, B. G., Rousakis, T. C., and Karabinis, A. I. (2016). "Fatigue behavior of large-scale reinforced concrete beams strengthened in flexure with fiber-reinforced polymer laminates." *J. Compos. Constr*. DOI: 10.1061/(ASCE)CC.1943-5614.0000689, 04016035.

597 Chen, C., and Cheng, L. J. (2016). "Fatigue behavior and prediction of NSM
598 CFRP-strengthened reinforced concrete beams." *J. Compos. Constr*. DOI:
599 10.1061/(ASCE)CC.1943-5614.0000691, 04016033.
600 Ekenel, M., Rizzo, A., Myers, J. J., and Nanni, A. (2006). "Flexural fatigue behavior of
601 reinforced concrete beams strengthened with FRP fabric and precured laminate
602 systems." *J. Compos. Constr*, 10(5), 433-442.
603 El-Hacha, R., Wight, G. R., and Green, M. F. (2001). "Prestressed fiber-reinforced
604 polymer laminates for strengthening structures." *Pro Struct. Eng. Mater.*, 3(2),
605 111-121.
606 Erki, M. A., and Meier, U. (1999). "Impact loading of concrete beams externally
607 strengthened with CFRP laminates." *J. Compos. Constr*, 3(3), 117-124.
608 Gussenhoven, R., and Brena, S. F. (2005). "Fatigue behavior of reinforced concrete
609 beams strengthened with different FRP laminate configurations." In *FRP*
610 *Reinforcement for Concrete Structures, SP230-SP236*, pp. 613-630*,* American
611 Concrete Institute, Kansas City.
612 Heffernan, P. J., Erki, M. A., and DuQuesnay, D. (2004). "Stress redistributions in a
613 cyclically loaded reinforced concrete beam." *ACI Struct. J.*, 101(2), 261-268.
614 Holmen, J. O. (1982). "Fatigue of concrete by constant and variable amplitude loading."
615 In *Fatigue of Concrete Structures, SP,* pp. *75-74*, pp. 71–110*,* American Concrete
616 Institute, Detroit.
617 Hull, D. (1981). *An Introduction to Composite Materials*, Cambridge University Press,
618 London.

619 Kim, Y. J., Longworth, J. M., Wight, R. G., and Green, M. F. (2010). "Punching shear of
620 two-way slabs retrofitted with prestressed or non-prestressed CFRP sheets." *J.*
621 *Reinf. Plast. Compos.*, 29(8), 1206-1223.
622 Larson, K. H., Peterman, R. J., and Rasheed, H. A. (2005). "Strength-fatigue behavior of
623 fiber reinforced polymer strengthened prestressed concrete T-beams." *J. Compos.*
624 *Constr*, 9(4), 313-326.
625 Masoud, S., Soudki, K., and Topper, T. (2005). "Postrepair fatigue performance of
626 FRP-repaired corroded RC beams: Experimental and analytical investigation." *J.*
627 *Compos. Constr*, 9(5), 441-449.
628 Meier, U. (1995). "Strengthening of structures using carbon fibre/epoxy composites."
629 *Constr. Build. Mater.*, 9(6), 341-351.
630 Miner, M. A. (1945). "Cumulative damage in fatigue." *J. Appl. Mech.*, 12, 159-164.
631 Ministry of Transport of the People's Republic of China (MTPRC). (2004). "Code for
632 design of highway reinforced concrete and prestressed concrete bridges and
633 culverts." *People*'s Communication Press, Beijing, 23-27.
634 Mukherjee, A., and Rai, G. L. (2009). "Performance of reinforced concrete beams
635 externally prestressed with fiber composites." *Constr. Build. Mater.*, 23(2),
636 822-828.
637 Nanni, A., Bakis, C. E., O'Neil, E. F., and Dixon, T. O. (1996). "Performance of FRP
638 tendon-anchor systems for prestressed concrete structures." *PCI J.*, 41(1), 34-44.
639 Nanni, A., Tanigaki, M., and Hasuo, K. (1992). "Bond anchorage of pretensioned FRP
640 tendon at force release." *J. Struct. Eng.*, 118(10), 2837-2854.

641 Papakonstantinou, C. G., Petrou, M. F., and Harries, K. A. (2001). "Fatigue behavior of
642 RC beams strengthened with GFRP sheets." *J. Compos. Constr*, 5(4), 246-253.
643 Quattlebaum, J. B., Harries, K. A., and Petrou, M. F. (2005). "Comparison of three
644 flexural retrofit systems under monotonic and fatigue loads." *J. Bridge Eng.*,
645 10(6), 731-740.
646 Rosenboom, O. A., and Rizkalla, S. M. (2005). "Fatigue behavior of prestressed concrete
647 bridge girders strengthened with various CFRP systems." In *FRP Reinforcement*
648 *for Concrete Structures,* pp. *SP230-SP235*, pp. 597-612*,* American Concrete
649 Institute, Kansas City.
650 Rösler, J., Bäker, M., and Harders, H. (2007). *Mechanical Behaviour of Engineering*
651 materials,, Springer Verlag Publishing, Berlin, Germany.
652 Saadatmanesh, H., and Malek, A. M. (1998). "Design guidelines for flexural
653 strengthening of RC beams with FRP plates." *J. Compos. Constr*, 2(4), 158-164.
654 Shahawy, M., and Beitelman, T. E. (1999). "Static and fatigue performance of RC beams
655 strengthened with CFRP laminates." *J. Struct. Eng.*, 125(6), 613-621.
656 Sherif, E. T., Cahit, O., Ayman, O., and Mohsen, S. (2001). "Static and fatigue analyses
657 of RC beams strengthened with CFRP laminates." *J. Compos. Constr.*, 4(5),
658 258-267.
659 Sika CarboDur. (2005). "Product data sheet: Carbon fiber laminate for structural
660 strengthening.", p. 04.2005 Ed., ⟨http://ca01.webdms.sika.com/fileshow.do?
661 documentID=57⟩.

662 Sika CarboStress.. (2014). “Refurbishment: Structural strengthening with Sika systems.”,
663 p. 12.2014 Ed., ⟨https://www.sika.com/en/system/search.html?q=
664 SikaServicesAG-Refurbishment-Structural_Strengthening_With_Sika_Systems⟩.
665 Su, Y., Wu, C. Q., and Griffth, M. C. (2011). “Modeling of the bond-slip behavior in
666 FRP reinforced masonry.” *Constr. Build. Mater.*, 25(1), 328-334.
667 Toutanji, H., Zhao, L., Deng, Y., Zhang, Y., and Balaguru, P. (2006). “Cyclic behavior of
668 RC beams strengthened with carbon fiber sheets bonded by inorganic matrix.” *J.*
669 *Mater. Civ. Eng.*, 18(1), 28-35.
670 Triantafillou, T. C., and Deskovic, N. (1991). “Innovative prestressing with FRP sheets:
671 Mechanics of short-term behavior.” *J. Eng. Mech.*, 117(7), 1652-1672.
672 Wang, W. W., and Dai, J. G. (2013). “Self-stressed steel fiber reinforced concrete as
673 negative moment connection for strengthening of multi-span simply-supported
674 girder bridges.” *Adv. Struct. Eng.*, 16(6), 1113–1127.
675 Wang, W. W., Dai, J. G., and Harries, K. A. (2013). “Intermediate crack-induced
676 debonding in RC beams externally strengthened with prestressed FRP laminates.”
677 *J. Reinf. Plast. Compos.*, 32(23), 1842–1857.
678 Wang, W. W., Dai, J. G., Harries, K. A., and Bao, Q. H. (2012). “Prestress losses and
679 flexural behavior of reinforced concrete beams strengthened with posttensioned
680 CFRP sheets.” *J. Compos. Constr*, 16(2), 207-216.
681 Wang, W. W., Dai, J. G., Harries, K. A., and Zhang, L. (2014). “Prediction of prestress
682 losses in RC beams externally strengthened with prestressed CFRP sheets/plates.”
683 *J. Reinf. Plast. Compos.*, 33(8), 699–713.

684 Wight, R. G., and Erki, M. A.. (2003). “Prestressed CFRP sheets for strengthening
685 concrete slabs in fatigue.” *Adv. Struct. Eng.*, 6(3), 175-182.
686 Wight, R. G., Green, M. F., and Erki, M. A. (2001). “Prestressed FRP sheets for
687 poststrengthening reinforced concrete beams.” *J. Compos. Constr.*, 5(4), 214–220.
688 Xie, J. H., Huang, P. Y., and Guo, Y. C. (2012). “Fatigue behavior of reinforced concrete
689 beams strengthened with prestressed fiber reinforced polymer.” *Constr. Build.*
690 *Mater.*, 27(1), 149-157.
691 Yu, T. L., Li, C. Y., Lei, J. Q., and Zhang, H. X. (2011). “Fatigue of concrete beams
692 strengthened with glass-fiber composite under flexure.” *J. Compos. Constr*, 15(4),
693 557-564.
694

Table 1. Summary of Test Specimens

Beam ID	CFRP sheet	Prestress level (%)	Fatigue load (kN)		P_u (kN)	P_{min}/P_u	P_{max}/P_u	Fatigue life
			P_{max}	P_{min}				
SB-1	-	-	-	-	47.3	-	-	-
SB-2	One ply with cross sectional area 23.38mm^2	-	-	-	77.9	-	-	-
SB-3		60	-	-	85.3	-	-	-
SB-4	Two plies with cross sectional area 46.76mm^2	30	-	-	115.0	-	-	-
FB-1	-	-	19.8	5.9	-			>2,000,000
FB-2	One ply with cross sectional area 23.38mm^2	-	31.2	9.3	-	0.12	0.4	>2,000,000
FB-3		60	34.1	10.2	-			>2,000,000
FB-4		60	42.7	12.8	-			1,730,000
FB-5	Two plies with cross sectional area 46.76mm^2	30	57.5	17.3	-	0.15	0.5	1,890,000

Table 2. Parameters for Eq. (2)

Parameter	k	K_0	Δ	d
Ribbed steel reinforcement	4	2.34×10^{15}	0.657	0
Smooth steel reinforcement	3.5	1.08×10^{14}	0.625	0

Table 3. Comparisons between Tested Life and Predicted Life

Reference	Beam ID	E_c (GPa)	E_s (GPa)	E_f (GPa)	P_{max}/P_u	P_{min}/P_u	N_t (cycles)	N_{pu} (cycles)	N_{pd} (cycles)	N_{pu}/N_t	N_{pd}/N_t
Papakons-antinou (2001)	S-2	34.5	200	72.4	0.63	0.03	880,000	642,879	385,443	0.73	0.44
	S-5	34.5	200	72.4	0.66	0.05	800,000	635,325	380,914	0.79	0.48
	S-6	34.5	200	72.4	0.87	0.06	126,000	121,258	72,701	0.96	0.58
	S-9	34.5	200	72.4	0.78	0.04	235,000	187,634	112,497	0.80	0.48
	S-10	34.5	200	72.4	0.6	0.04	685,000	599,712	359,562	0.87	0.52
Heffernan (2004)	M-CFa	34.5	210	233	0.7	0.2	900,000	1,312,025	968,186	1.45	1.08
	M-CFb	34.5	210	233	0.7	0.2	890,000	1,312,025	968,186	1.47	1.09
	H-CFa	34.5	210	233	0.8	0.2	340,000	531,520	392,225	1.56	1.15
	H-CFb	34.5	210	233	0.8	0.2	390,000	531,520	392,225	1.36	1.01
Quattleba-um (2005)	C-L(b)	31.5	200	216	0.59	0.16	587,000	666,240	460,341	1.13	0.78
	C-H	31.5	200	216	0.59	0.15	523,000	618,026	427,027	1.18	0.82
	N-H	31.5	200	216	0.58	0.16	800,000	629,553	434,992	0.79	0.54
Toutanji (2006)	3FI-9	36	210	228	0.6	0.1	259,432	213,064	98,289	0.82	0.38
	3FI-10	36	210	228	0.6	0.1	314,728	213,064	98,289	0.68	0.31
	3FI-11	36	210	228	0.6	0.1	197,954	213,064	98,289	1.08	0.50
	3FI-12	36	210	228	0.7	0.1	74,383	81,968	37,813	1.10	0.51
	3FI-13	36	210	228	0.7	0.1	74,579	81,968	37,813	1.10	0.51
Barnes (1999)	3	34.5	200	135	0.43	0.04	508,500	491,025	326,469	0.97	0.64
	4	34.5	200	135	0.35	0.04	1,889,200	1,495,732	994,473	0.79	0.53
Xie (2012)	P_{h1}	35.2	226	240	0.6	0.06	227,030	195,430	109,635	0.86	0.48
	P_{h2}	35.2	226	240	0.6	0.06	250,071	195,430	109,635	0.78	0.44
	P_{h3}	35.2	226	240	0.6	0.06	377,688	195,430	109,635	0.52	0.29
Yu (2011)	LJP-2	25.5	210	30.2	0.39	0.07	1,780,000	1,932,372	1,814,250	1.09	1.02
	LJP-3	25.5	210	30.2	0.51	0.07	420,789	536,258	503,477	1.27	1.20
	LJP-4	25.5	210	30.2	0.62	0.07	130,000	144,073	135,266	1.11	1.04
	LJP-5	25.5	210	30.2	0.75	0.07	54,000	65,873	61,846	1.22	1.15
Present work	FB-4	35.6	200	258.9	0.5	0.15	1,730,000	1,772,354	1,462,951	1.02	0.85
	FB-5	35.6	200	258.9	0.5	0.15	1,890,000	1,682,450	1,156,418	0.89	0.61
Mean										1.02	0.69
COV										0.25	0.28

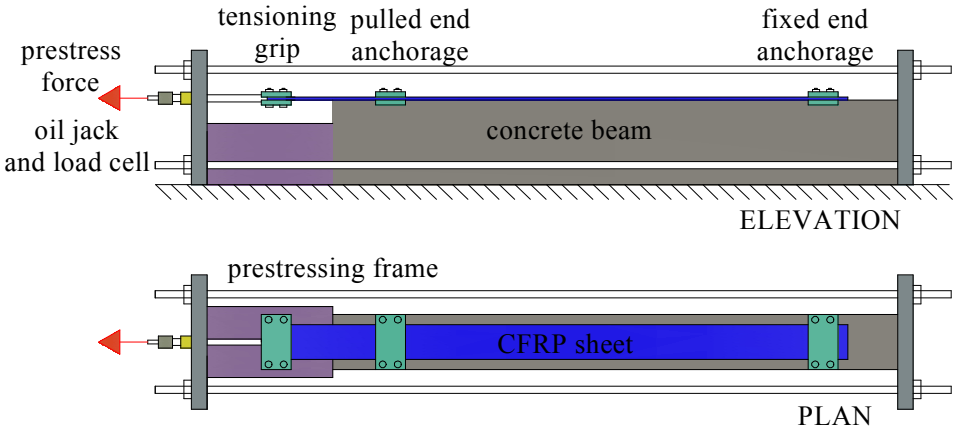

Fig. 1. Post-tensioning system for pre-stressed CFRP sheet

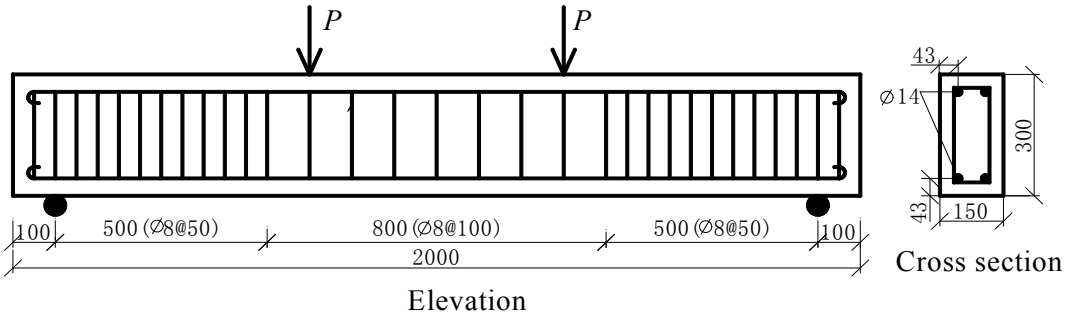

Fig. 2. Details of test specimen (unit in mm)

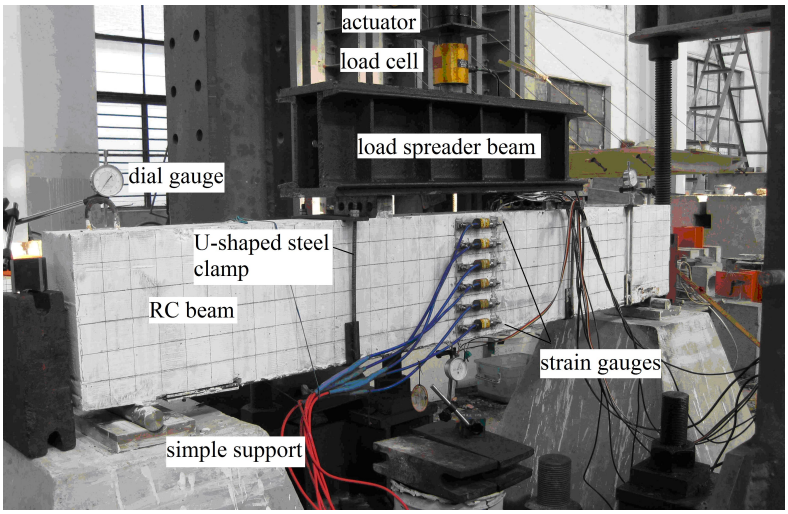

Fig. 3. Test setup

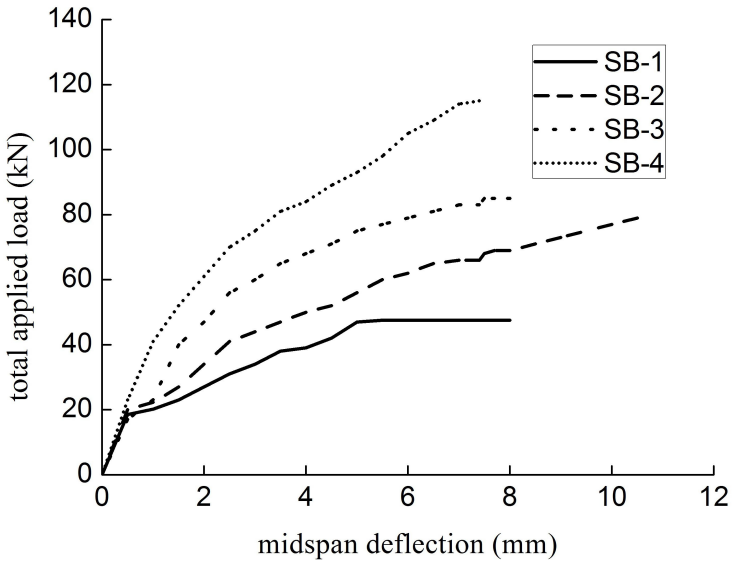

Fig. 4. Load-displacement responses of static test beams

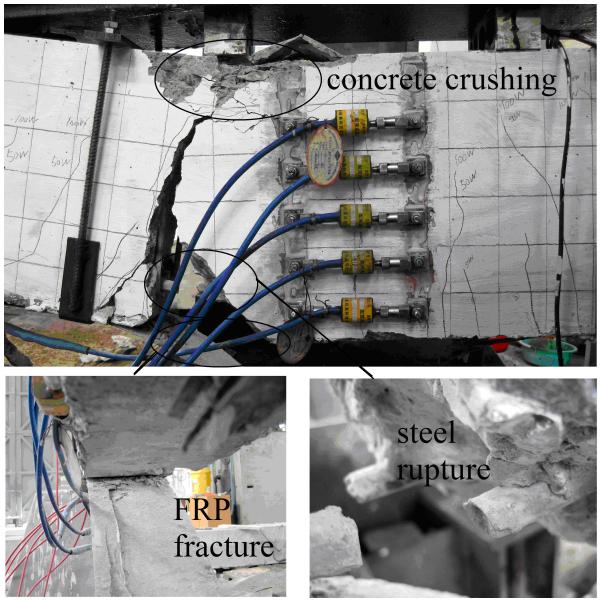

(a)

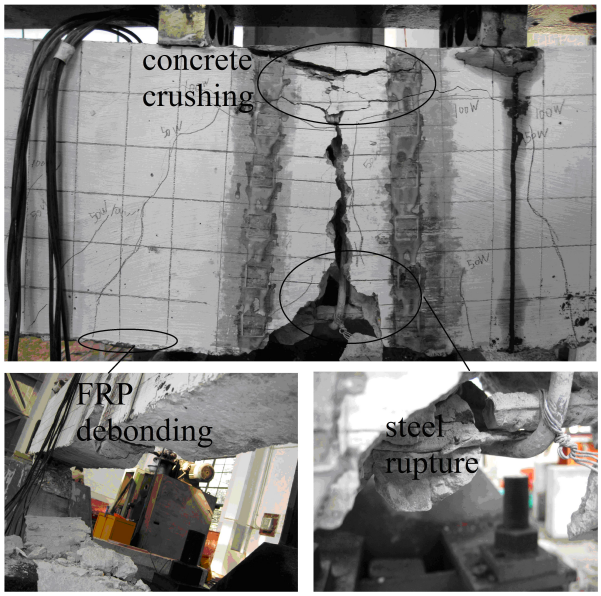

(b)

Fig. 5. Fatigue failure modes: (a) FB-4; (b) FB-5

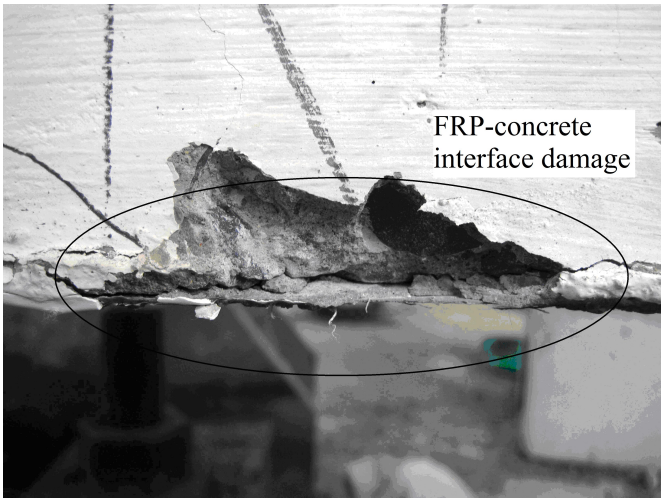

(a)

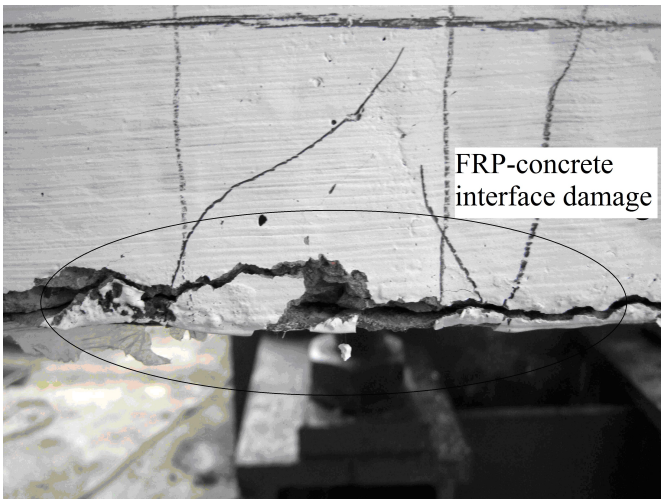

(b)

Fig. 6. FRP-concrete interface damage: (a) FB-4; (b) FB-5

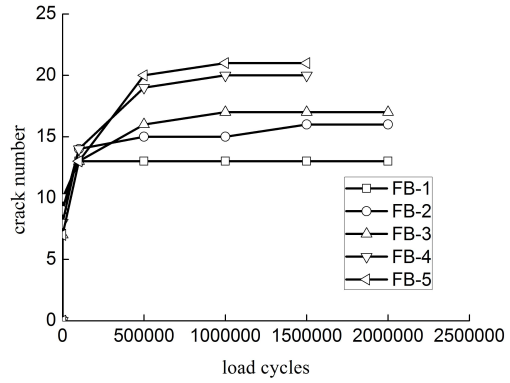

(a)

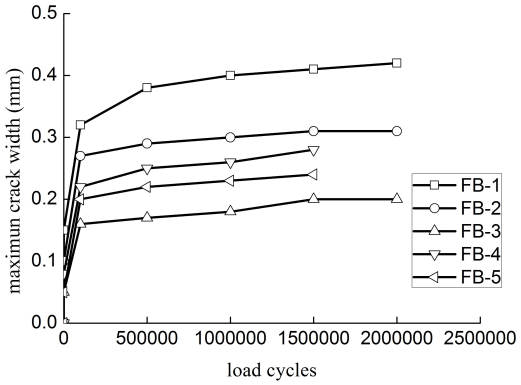

(b)

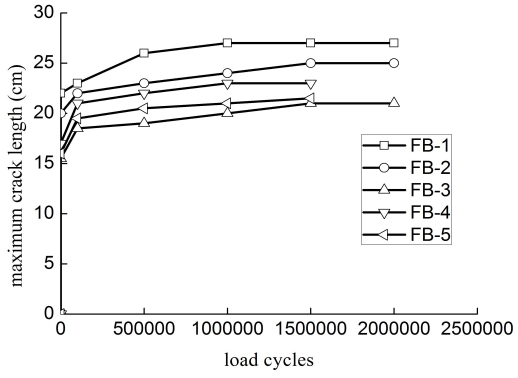

(c)

Fig. 7. Crack development versus load cycles at the corresponding upper limit fatigue load of each specimen: (a) Crack number; (b) Maximum width of crack; and (c) Maximum length of crack

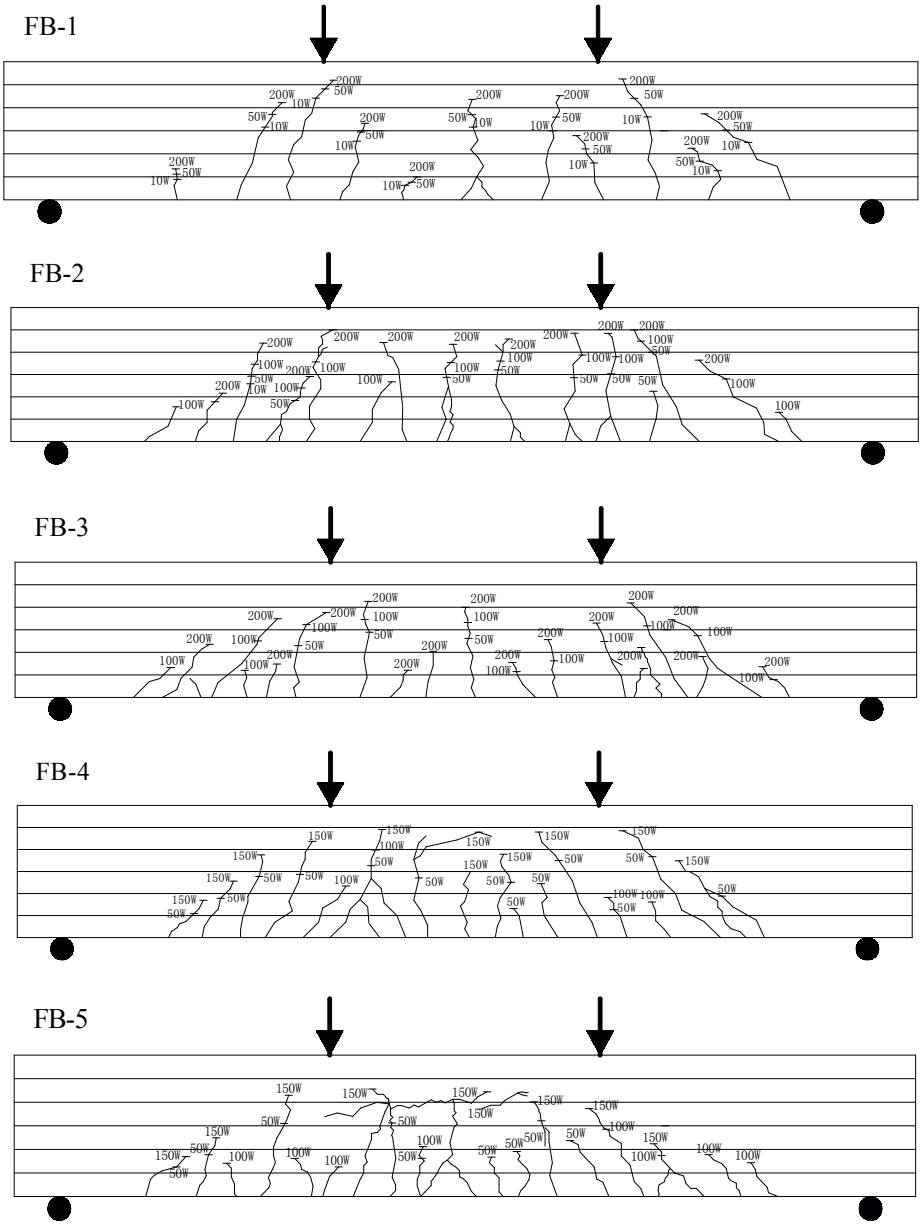

Fig. 8. Cracks distribution maps of all fatigue tested specimens (1W = 10,000 loading cycles)

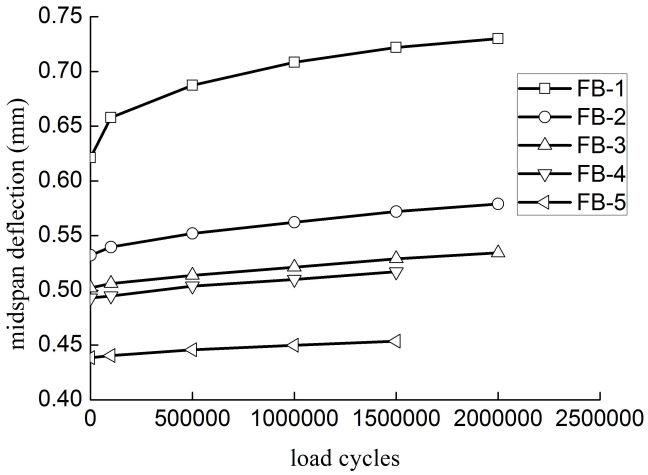

Fig. 9. Mid-span deflections versus load cycles at the given load of 19.8 kN

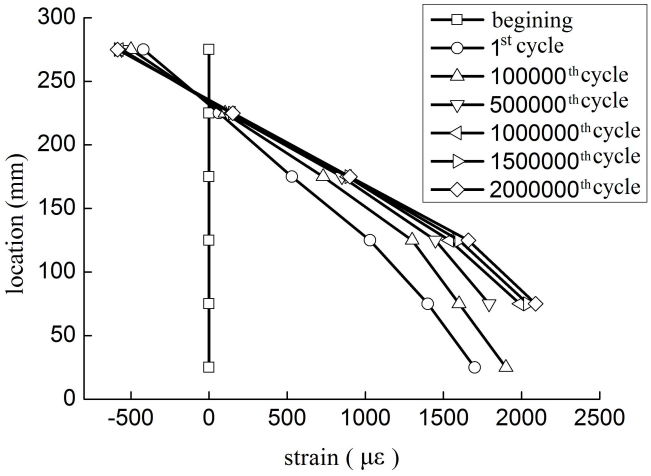

Fig. 10. Sectional strain distribution versus load cycles at the given load of 34.1 kN (FB-3)

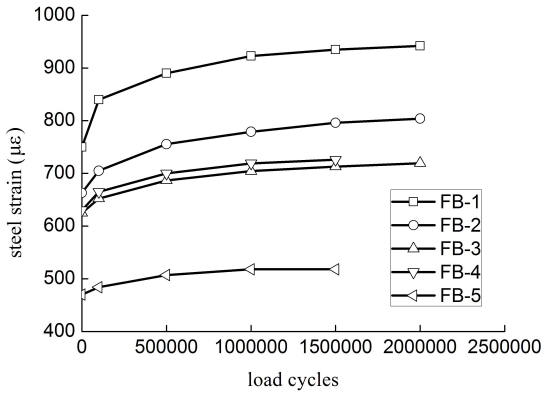

(a)

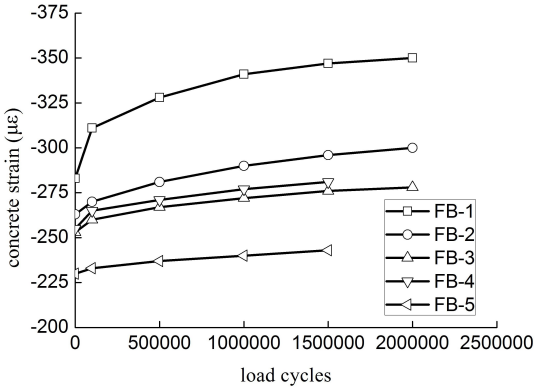

(b)

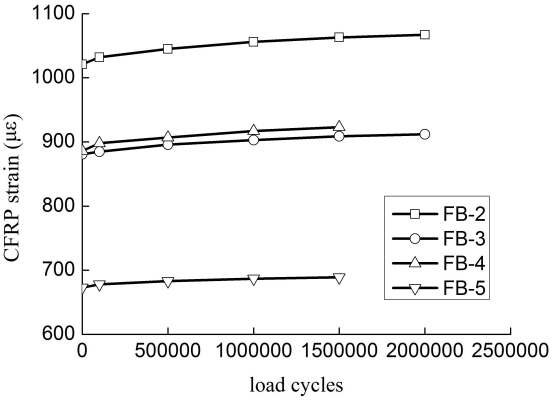

(c)

Fig. 11. Strains versus load cycles at the load of 19.8 kN: (a) Steel reinforcement; (b) Concrete; and (c) CFRP sheet

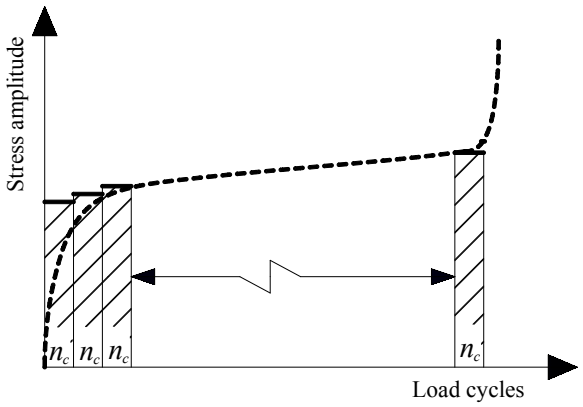

Fig. 12. Discretization of steel stress amplitudes

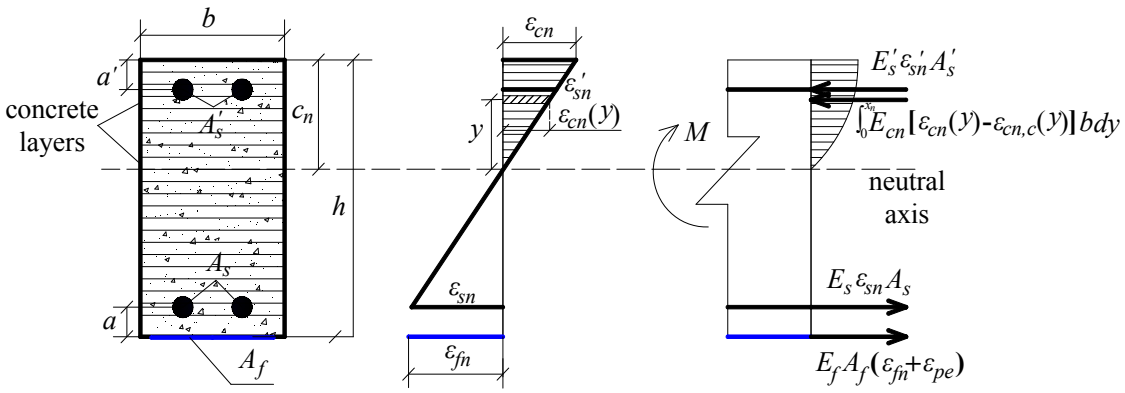

Fig. 13. Strain-stress distribution at the main cracked section

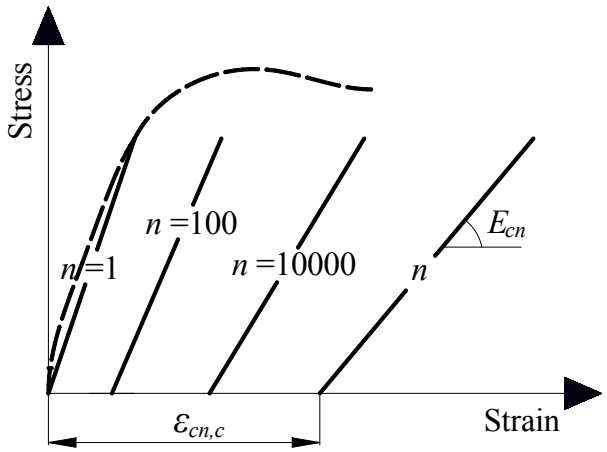

Fig. 14. Stress-stain relationship for concrete

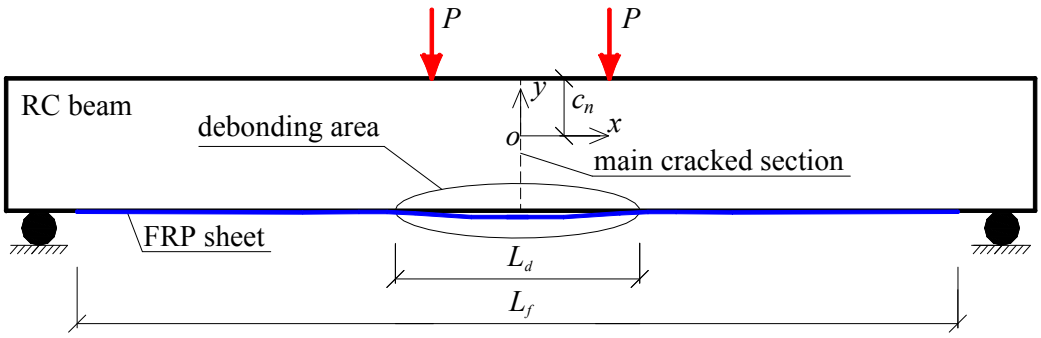

Fig. 15. The mechanical behavior of FRP sheet during the fatigue loading

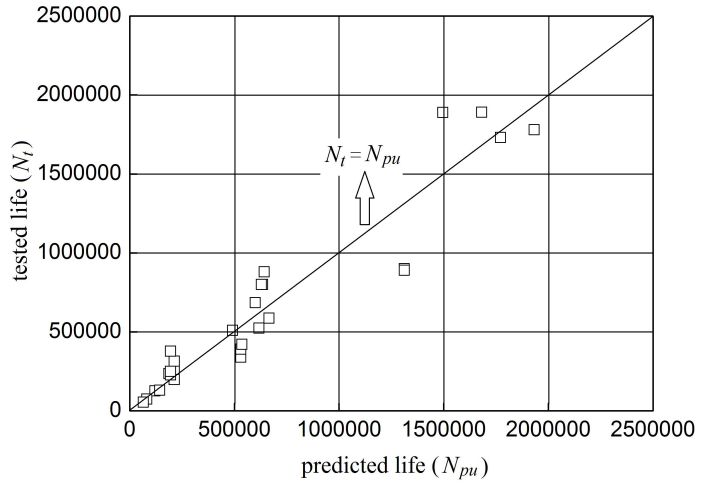

(a)

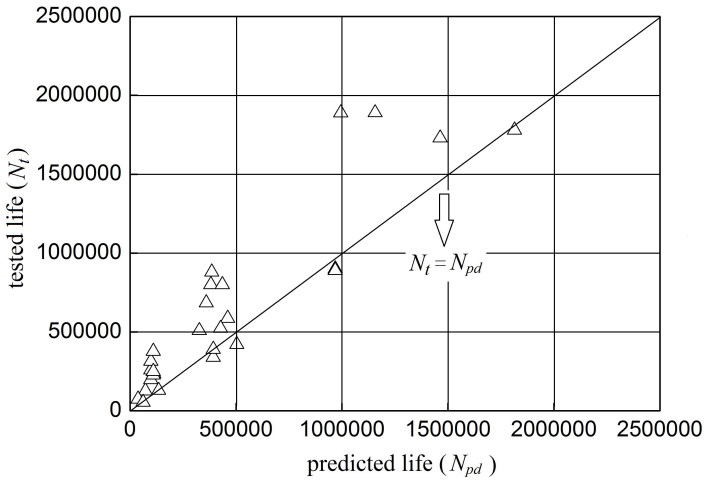

(b)

Fig. 16. Tested life versus predicted life for two limit states: (a) state 1: $L_d = 0$; (b) state 2: $L_d = L_f$